Lightweight and Compliant Long Reach Aerial Manipulator for Inspection Operations

A. Suarez, P. Sanchez-Cuevas, M. Fernandez, M. Perez, Guillermo Heredia, and Anibal Ollero

Abstract— **The proximity between the multirotor blades and the environmental obstacles restricts the application of aerial manipulators in inspection tasks due to the risk of impacts, the limitation in the reach of the arm, and the physical interactions. This paper presents a long reach aerial manipulator consisting of a hexarotor platform equipped with a 2-DOF compliant joint arm attached at the tip of a one-meter-length link in passive pendulum configuration. The arm integrates magnetic encoders for force/torque estimation-control based on joint deflection, a range sensor in the forearm link for measuring the distance to the contact point, and a camera for visual inspection. A 2-DOF wearable exoskeleton interface has been developed, allowing the teleoperation of the arm with visual feedback in a more intuitive way. The paper also covers the kinematics and dynamics of the aerial manipulator, including the dynamics of the flexible long reach link. The developed system has been evaluated in test-bench and in outdoor flight tests.**

I. INTRODUCTION

In recent years the development of autonomous aerial robots capable of physical interaction is catching much interest in robotic research [1][2]. Aerial robots with integrated robotic manipulators, known as *aerial manipulators* [3][4][5], offer strong potentialities for applications as the inspection and maintenance of industrial facilities and infrastructures, aerial power lines, moving objects, and taking samples of material from areas that are difficult to access.

Safety and reliability are important requirements in aerial manipulation since the mechanical or environmental damages derived from unexpected interactions during the operation on flight (impacts, grabbing situations, motion constraints, wind disturbances) may suppose the partial destruction of the robot and the risk of severe consequences in certain facilities, like fires in chemical plants. Considering an aerial manipulator performing an inspection or maintenance task in outdoors [6][7], safety can be improved increasing the distance between the aerial platform and the obstacles, so the risk of impact of the blades of the multirotor [4][8] or helicopter [9] is low. This is highly convenient taking into account that the reach of the manipulator is typically within the perimeter of the blades of the aerial platform [3]–[9]. Additionally, the forces-torques associated to the physical interaction on flight may destabilize the attitude controller of the vehicle [10][11]. In this sense, the mechanical compliance [7][12][13] increases the tolerance of the manipulator to overloads or impacts, allowing the control of contact forces in terms of joint deflection [14][15].

Some works have used teams of UAVs that cooperatively carry platforms with end effectors or arms to extend the reach

A. Suarez (asuarezfm@us.es), P. J. Sanchez-Cuevas (psanchez16@us.es), M. J. Fernandez, M. Perez, G. Heredia (guiller@us.es), and A. Ollero (aollero@us.es) are with the Robotics, Vision and Control Group at the University of Seville, Spain.

of the aerial manipulator. The position and orientation of the platform is set controlling the position in space of the UAVs. A towed-cable system with a platform connected with cables to three quadrotors has been presented in [16]. A platform which consists of a rigid frame and multiple quadrotors that are connected to the frame through rigid bars with passive spherical joints is proposed in reference [17]. Although these configurations increase the payload of the system, they also have operational limitations coming from the large open space needed for the multiple quadrotors to fly safely.

The aerial manipulator described in this paper is based on the prototypes developed in our previous work. The idea of using a flexible long reach link for extending the workspace of a dual arm manipulator and for improving safety during the physical interactions on flight was firstly introduced in [18], considering in that case the dual arm system described in [19]. This new prototype incorporates a passive joint at the base of the long reach link, using a modified version of the compliant arm presented in [14] that allows the estimation and control of the contact force/impedance from the Cartesian deflection, as defined in [15]. This long reach manipulator (LRM) is suitable for several tasks in narrow spaces: pipe inspection (Figure 1), sensor installation, corrosion repair, or insulation of leaks.
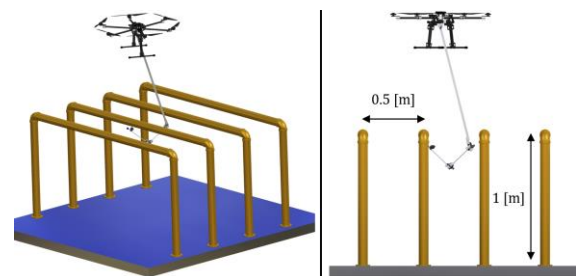

Figure 1. Application of long reach aerial manipulator to pipe inspection. The long reach link allows the operation in narrow spaces and the detection of leaks at the bottom of the pipes using an eye-in-hand camera.

The main contribution of this work is the development of a compliant joint, long reach aerial manipulator designed for inspection operations and its experimental validation in test-bench and outdoor flight tests. The aerial manipulator consists of a 2-DOF compliant joint arm which is attached at the tip of a 1 m length link that rotates freely with respect to the base of the multirotor, similarly to a pendulum. The arm integrates several sensors that allow the position and force control of the arm. A wearable exoskeleton interface with visual feedback is also developed, in such a way that the operation of the arm results more intuitive for an untrained operator. The kinematic and dynamic models of the robot are presented, proposing a UAV-LRM control scheme. The experimental results show the take-off and landing maneuvers, the response to impacts, the force control, and the teleoperation with visual feedback.

The rest of the paper is organized as follows. Section II describes the compliant joint, long reach aerial manipulator along with the exoskeleton interface. Section III presents the kinematic and dynamic models of the aerial robot, including the dynamics of the flexible link. The proposed control system is described in Section IV, showing the experimental results in Section V and the conclusions in Section VI.

II. SYSTEM DESCRIPTION

A. Compliant Joint, Long Reach Aerial Manipulator

The developed long reach aerial manipulator consists of three components: the multirotor platform, the flexible long reach link attached at the base of the UAV through a passive joint in pendulum configuration, and the compliant joint arm placed at the tip of the link. A picture of the prototype can be seen in Figure 2, summarizing its specifications in Table 1. The aerial platform is a hexarotor manufactured by Drone Tools, equipped with a PixHawk autopilot. The long reach link is a 1 m length flat profile section of anodized aluminum supported by a pair of igus® EFOM-08 flange bearings. An 8 mm Ø crossing shaft rigidly attached to the base of the multirotor allows the free rotation of the link similarly to a pendulum, measuring the angle with a magnetic encoder. The sensors integrated in the arm are indicated in Table 2.
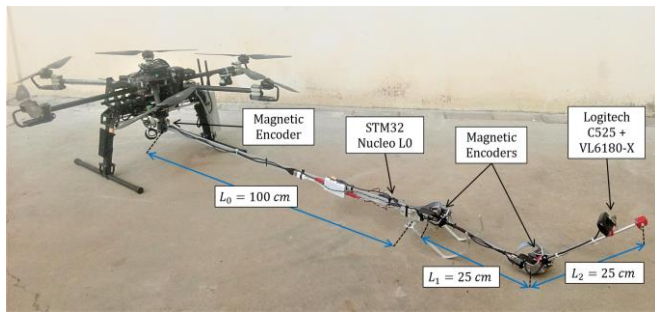

Figure 2. Compliant joint, long reach aerial manipulator.

Table 1. Specifications of the compliant joint, long reach aerial manipulator.

	Weight / Payload [kg]	3.4 / 2.5
Aerial Platform	Flight time [min]	~30 (no load)
	Batteries (2 kg, included)	6S, 7000 mAh
Flexible Link + Integration frame	Dimensions [mm]	1000 × 25 ×2
	Weight [kg]	0.27
Compliant Joint Arm	Rotation range [°]	±120
	Weight / Lift load [kg]	0.5 / 0.2
	Link lengths [m]	0.25 / 0.25
	Joint stiffness [Nm/rad]	1.5 / 1.3

Table 2. Sensor devices integrated in the compliant arm.

Sensor	Range	Accuracy	Application
AS5048 magnetic encoder	±180°	0.2°	Deflection measurement in compliant joints, force torque estimation/control
VL6180X-SATEL ToF laser sensor	150 mm	3 mm	Measurement of distance from tool center point to the contact point
Logitech C525 camera	-	640×480 pixels	Visual inspection, eye-in-hand camera

One of the main features of this manipulator is the passive joint at the base of the pendulum. It prevents that the external wrenches generated during the physical interactions between the environment and the aerial manipulator are introduced as a torque in the pitch angle at the base of the multirotor. Instead, the components of the interaction wrenches contained in the plane orthogonal to the rotation axis of the joint are introduced as a force at the UAV base, whereas the components parallel to this axis will cause a deflection in the flexible link.

B. Wearable Exoskeleton Interface

The exoskeleton interface depicted in Figure 3 consists of an anodized aluminum frame structure manufacturing using standard 20 × 2, 25 × 2, and 30 × 2 mm flat profiles bended in such a way that they can fit as a backpack, supported over the shoulders and attached at the hip. The forearm and upper arm links are supported by igus® EFOM-08 flange bearings that allow the rotation of the shoulder and elbow joints, using the same magnetic encoders that in the compliant arm to measure the rotation angle. Two push-buttons have been included in a handle grasped by the user, connected to the wrist through a spherical joint. These buttons can be used to exert a pushing-pulling force with the compliant arm once the end effector is close to the inspection point. The development of this device is motivated by the convenience to facilitate the teleoperation of the inspection arm for an untrained operator. Section V-C will demonstrate its application along with a visual interface.
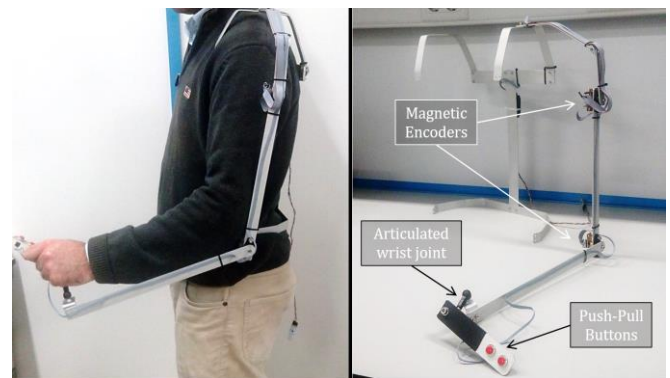

Figure 3. Wearable exoskeleton interface for arm teleoperation.

C. Hardware/Software Architecture

The developed aerial manipulator can be decomposed in two main subsystems: the aerial platform and the compliant joint LRM. The hardware components and the architecture is represented in Figure 4. The hexarotor integrates the PixHawk autopilot with the PX4 flight stack. The autopilot is connected to the Intel Nuc PC through a serial port. The communication between the two devices is based on the MAVROS protocol, whereas the mavros package of the Robot Operating System (ROS) is used for logging the data of interest (see Sections V-A,B). The components of the LRM are two Herkulex servos, three magnetic encoders for measuring the deflection of the joints and the rotation of the pendulum, and the camera and range sensors for the teleoperation. A STM32Nucelo L0 board reads all the sensors and sends a single data packet to the Intel NUC through the serial interface at 200 Hz. The execution of the experiment is managed from a Ground Control Station through SSH sessions to the computer board.
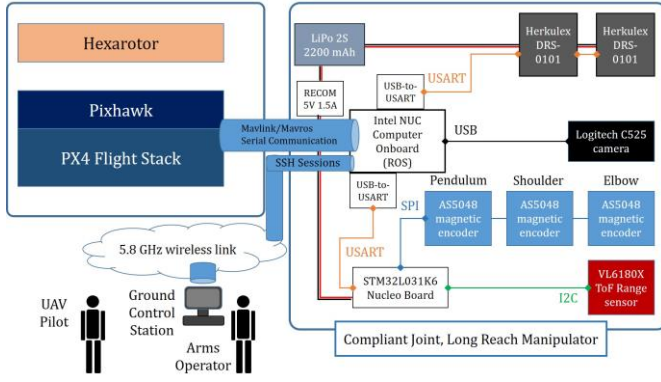
Figure 4. Hardware components and architecture of the aerial manipulator.

III. MODELING

A. Kinematics

The reference frames, position vectors, joint variables and link lengths of the developed long reach aerial manipulator are represented in Figure 5. Here, $\{E\}$, $\{B\}$ and $\{0\}$ are the Earth fixed frame, the UAV based frame, and the manipulator base frame, respectively. The position and orientation of the UAV are denoted by $r = [x, y, z]^T$ and $\eta = [\varphi, \theta, \psi]^T$. The rotation angle of the pendulum is represented by q_0, whereas q_1 and q_2 are the shoulder and elbow pitch joints of the compliant arm. The position and orientation of the arm frame relative to the UAV base frame are given by the transformation matrix:

$$^{B}T_0 = \begin{bmatrix} cos(q_0) & 0 & sin(q_0) & -L_0 sin(q_0) \\ 0 & 1 & 0 & 0 \\ -sin(q_0) & 0 & cos(q_0) & -L_0 cos(q_0) \\ 0 & 0 & 0 & 1 \end{bmatrix} \quad (1)$$

The position of the tool center point (TCP) in the Earth fixed frame depends on the three joint angles and on the heading and position of the aerial platform. Assuming hovering state ($\varphi = \theta = 0$) in the aerial platform, it is obtained as follows:

$$^{E}r_{TCP} = \begin{bmatrix} cos(\psi) \cdot \rho \\ sin(\psi) \cdot \rho \\ -\gamma \end{bmatrix} + \begin{bmatrix} x \\ y \\ z \end{bmatrix} \quad (2)$$

$$\rho = L_0 s(q_0) + L_1 s(q_0 + q_1) + L_2 s(q_0 + q_1 + q_2) \quad (3)$$

$$\gamma = L_0 c(q_0) + L_1 c(q_0 + q_1) + L_2 c(q_0 + q_1 + q_2) \quad (4)$$

Here $s(\alpha) = sin(\alpha)$ and $c(\alpha) = cos(\alpha)$. As done in [4], this work considers the rotation in the yaw angle of the aerial platform instead of using a third servo for this purpose [14].
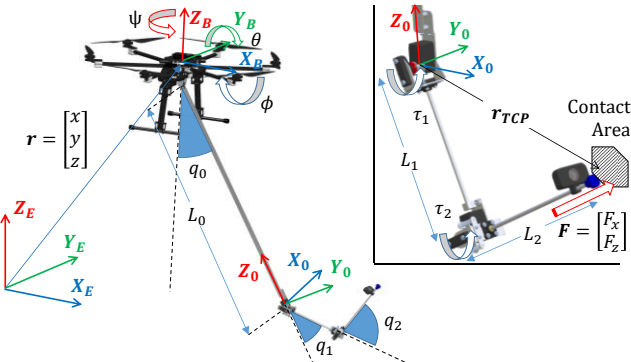

Figure 5. Kinematic model of the long reach aerial manipulator.

B. Dynamics

The dynamic model of the developed complaint joint, long reach aerial manipulator can be derived from the Lagrangian and the generalized equation of the forces and torques:

$$\frac{d}{dt}\left\{\frac{\partial L}{\partial \dot{\xi}}\right\} - \frac{\partial L}{\partial \xi} = \Gamma \; ; \; L = K_{UAV} + K_{LRM} - (V_{UAV} + V_{LRM}) \; (5)$$

Here L is the Larangian, defined as the difference between the kinetic (K_{UAV}, K_{LRM}) and potential (V_{UAV}, V_{LRM}) energy of the system, comprising the energy of the UAV and the long reach manipulator. The vector of generalized coordinates ξ includes the position and attitude of the aerial platform and the joint variables, and the generalized force vector Γ contains the wrenches acting over the platform along with the arm torques:

$$\xi = [r^T \quad \eta^T \quad q_0 \quad q_1 \quad q_2 \quad \theta_1 \quad \theta_2]^T \in \Re^{11} \quad (6)$$

$$\Gamma = [F^T \quad \tau^T \quad \tau_0 \quad \tau_1 \quad \tau_2 \quad \tau_{1,m} \quad \tau_{2,m}]^T \in \Re^{11} \quad (7)$$

Here q_0 is the rotation angle of the passive joint, θ_1 and θ_2 are the angular position of the arm servos, whereas q_1 and q_2 area the angular position of the output links. Both variables are related through the joint deflection angle $\Delta\theta_i$ [14][15]:

$$\Delta\theta_i = \theta_i - q_i \; ; \; \tau_{i,m} = k_i \Delta\theta_i + d_i \dot{\Delta\theta_i} \; ; \; i = \{1,2\} \; (8)$$

where k_i and d_i are the stiffness and damping of the i-th joint. The external wrenches acting over the manipulator can be estimated from the torque delivered by the motor, $\tau_{i,m}$, and the output link torque, τ_i [15]. Since the joint of the pendulum is passive, and its rotation axis is close to the center of mass of the multirotor, it can be assumed that $\tau_0 \cong 0$. This means that the long reach manipulator does not exert a torque in the pitch angle over the aerial platform, but a force in the XZ-axes, similarly to a tethered load. It is necessary to remark that this features contributes to increase safety during the operation on flight, as the passive joints of the pendulum prevents that the physical interactions on flight destabilize the aerial platform.

The kinetic and potential energy of the multirotor, K_{UAV} and V_{UAV}, are obtained from its mass m_{UAV} and inertia I_{UAV}:

$$K_{UAV} = \frac{1}{2}m_{UAV}\dot{r}^T\dot{r} + \frac{1}{2}\omega^T I_{UAV}^T \omega \; ; V_{UAV} = m_{UAV}gz \; (9)$$

The kinetic energy of the long reach manipulator, K_{LRM}, depends on the mass and inertia of each of its links, m_i and I_i, whereas the potential energy, V_{LRM}, is the sum of the gravity term and the elastic potential of the compliant joints:

$$K_{LRM} = \frac{1}{2}\sum_{i=0}^{2}\left\{m_i\left(^{E}\dot{r}_i\right)^T\left(^{E}\dot{r}_i\right) + \left(^{E}\omega_i\right)^T I_i^T\left(^{E}\omega_i\right)\right\} \; (10)$$

$$V_{LRM} = g\sum_{i=0}^{2} m_i z_i + \sum_{i=1}^{2} k_i(\Delta\theta_i)^2 \quad (11)$$

The dynamic model of the long reach aerial manipulator can be expressed in the usual matrix form:

$$M(\xi)\ddot{\xi} + C(\xi,\dot{\xi}) + G(\xi) + K(\xi) + D(\dot{\xi}) = \Gamma \quad (12)$$

where M is are the generalized inertia matrix, G represents the centrifugal and Coriolis terms, G is the gravity component, whereas K and D are the elastic and damping terms of the compliant joint, long reach manipulator. The dynamic model

defined by Equation (12) will be used by the UAV controller described in Section IV-A for compensating the oscillations of the passive pendulum and the reaction wrenches of the arm.

C. Flexible Long Reach Link Dynamics

The dynamic model described before can be extended to include the flexible link dynamics, although this is out of the scope of this paper. The effect of the link deflection is more relevant when an external force is applied or when the aerial platform is accelerated in the Y_B axis. The dynamics of the flexible link is derived from the Euler-Bernoulli beam theory [20], defining the deflection at a certain point $x \in [0, L_0]$ along the link as the sum of an infinite number of vibration modes, where each vibration mode is the product of a modal shape function $\varphi_i(x)$, and a generalized coordinate $\delta_i(t)$ that depends on the time. In practice, the most significant effect is associated to the first vibration mode in terms of amplitude and frequency range. The link deflection is the computed as:

$$w(t, x) = \sum_{i=1}^{\infty} \varphi_i(x) \delta_i(t) \; ; \; w(t, L_0) \cong \varphi_1(L_0) \delta_1(t) \quad (13)$$

The deflection at the tip, $w(t, L_0)$, can be measured using vision sensors installed at the base of the flexible link [18]. The response of the flexible link to an external force can be assimilated to a mass-spring-damper system as follows:

$$m_1^{FL} \ddot{\delta}_1(t) + d_1^{FL} \dot{\delta}_1(t) + k_1^{FL} \delta_1(t) = F_{ext}(t) \quad (14)$$

where m_1^{FL}, d_1^{FL}, and k_1^{FL} are the mass, damping and stiffness associated to the first vibration mode of the flexible link, and F_{ext} is the external force. In particular, the stiffness constant can be determined measuring the deflection obtained for a known force in static conditions, whereas the damping can be estimated from the natural response (free oscillation) of the tip. According to [20], the transfer function that relates the torque at the base of the flexible link with the flexible link deflection has positive zeros that may become unstable poles in a closed loop controller, complicating the position control.

IV. CONTROL

A. Coordinated UAV-Manipulator Control Scheme

The proposed long-reach aerial manipulator is intended to perform inspection operations and tasks requiring accurate position and force control at the end effector. The particular implementation will depend on the positioning system (GPS, laser tracking system, visual odometry, SLAM…) and on the way the operator specifies the desired inspection points. However, the control scheme should follow a scheme similar to the one represented in Figure 6, where the UAV position, heading, and thrust ($\boldsymbol{r}_{ref}$, ψ_{ref} and $\boldsymbol{U}$ in the diagram) are commanded in such a way that the manipulator is able to reach and exert the desired position and force.

The application of contact forces has associated two main effects over the robot. On the one hand, the component of the force in the forward direction will cause a recoil displacement in the passive joint until the equilibrium of forces is reached, that is, when the applied force $F_{x,ref}$ equals the projection in the X-axis of the gravity force.

$$F_{x,ref} = m_{LRM} \cdot g \cdot sin(q_0) \quad (15)$$

where m_{LRM} is the mass of the long reach manipulator, g is the gravity constant, and q_0 is the rotation of the pendulum joint. Note that the pushing or pulling force in this axis can be controlled indirectly through the relative position of the aerial platform w.r.t. the contact point, which determines the rotation angle q_0. On the other hand, the Z-axis component of the contact force should be compensated by the propellers, being possible to define an impedance behavior [10][11].
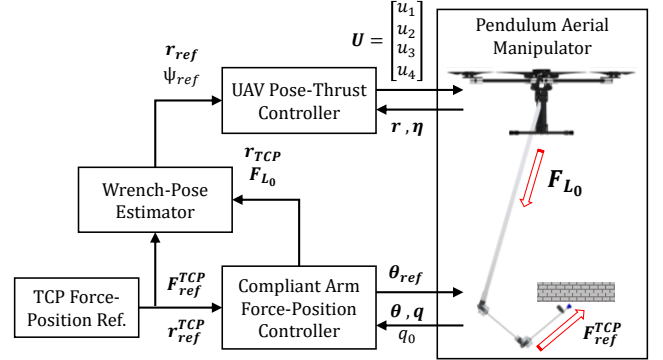

Figure 6. Coordinated UAV-long reach manipulator control scheme. The goal is to control the position and force of the tool center point of the arm. The pose and thrust of the UAV is adapted to achieve this reference.

The undesired oscillations introduced in the passive joint due to impacts or accelerations can be cancelled coordinating the motion of the robotic arm with the aerial platform, or well with any of these separately. However, as it will be seen in Section V-E, the ability of the compliant arm to attenuate the oscillations in the pendulum is limited since the mass and inertia of the arm is much lower than the mass/inertia of the long reach manipulator. This can be also derived comparing the kinetic and potential energy of the aerial platform and the manipulator given by Equations (9) – (11).

B. Force-Position Control Scheme

The contact force controller of the compliant joint arm is a modified version of the Cartesian impedance control scheme described in [15]. Unlike previous reference, where we used a vision system to measure the Cartesian deflection at the tool center point at 10 Hz update rate, in this work we integrated magnetic encoders in the joints to measure accurately the joint deflection at rates up to 1 kHz, improving the estimation and control of the forces and torques. In the following, the position vectors in the task space are defined in $\mathfrak{R}^2$, that is, in the $\boldsymbol{X_0 Z_0}$ plane, since the deflection is measured in the shoulder and elbow joints whose axes are orthogonal to this plane.

The force control is defined in the task space from the Cartesian deflection measured at the TCP, $\Delta \boldsymbol{l_{TCP}}$. This vector represents the deviation of the TCP position in a compliant joint arm w.r.t. the same position in an equivalent stiff joint arm, in such a way that the force exerted at the end effector is proportional to the deflection. That is:

$$\Delta \boldsymbol{l_{TCP}} = \boldsymbol{FK}(\boldsymbol{\theta}) - \boldsymbol{FK}(\boldsymbol{q}) \; ; \; \boldsymbol{F_{TCP}} = \boldsymbol{K_C} \Delta \boldsymbol{l_{TCP}} \quad (17)$$

Here $\boldsymbol{K_C} \in \mathfrak{R}^{2 \times 2}$ is the Cartesian stiffness matrix, defined in the following way [15]:

$$\boldsymbol{K_C} = (\boldsymbol{J^T})^{-1} \boldsymbol{K_p} \boldsymbol{J}^{-1} \; ; \; \boldsymbol{K_p} = diag\{k_1, k_2\} \quad (18)$$

where $K_p \in \Re^{2 \times 2}$ is the physical joint stiffness matrix, and $J \in \Re^{2 \times 2}$ is the Jacobian of the manipulator. Note that K_C is not diagonal in general. The virtual Cartesian stiffness will vary with the position of the manipulator due to the Jacobian.

The force/position control scheme implemented in the arm is depicted in Figure 7. The force error, that is, the difference between the reference and the force estimation given by Eq. (17) is taken as input by the force controller, giving as output the displacement of the TCP for correcting the force error. The joint position reference sent to the servos is obtained from the inverse kinematics, applied over the position vector r_{ref}, which is the sum of the force and position corrections, and the current TCP position obtained from the forward kinematics.

$$\theta_{ref} = IK(r_{ref}) = IK(\Delta r_F + \Delta r_P + FK(\theta)) \quad (19)$$

The position correction $\Delta r_P \in \Re^2$ is obtained integrating the velocity references provided by a joystick controlled by the operator of the arms. The force/position control modes can be switched simply enabling or disabling the force/position terms in Equation (19). This control scheme will be validated experimentally in Section V-D in a contact inspection task.
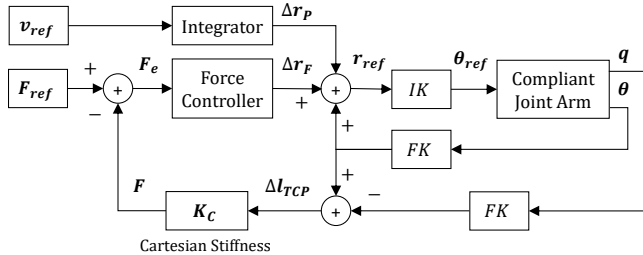

Figure 7. Force-position control scheme implemented in the compliant arm. The force is estimated from the Cartesian deflection Δl_{TCP} and stiffness K_C.

V. EXPERIMENTAL RESULTS

A. Takeoff and Landing

The aim of this experiment is to demonstrate that the long reach aerial manipulator is capable to perform the take-off and landing operations without needing a platform. Figure 8 shows a sequence of images corresponding to the landing operation taken from the video attachment. As it can be seen in Figure 2, a C-shaped aluminum frame structure is attached at the back of the compliant arm to prevent that the actuators are damaged during the maneuver. The evolution of the UAV position, velocity, attitude, and the rotation of the passive joint can be followed in Figure 9. The LRM lays initially in the floor almost horizontally, until the multirotor takes-off at t = 14 s. The take-off operation causes a 20 deg amplitude oscillation in the passive joint which remains until the tip of the LRM hits the floor at t = 40 s, when the UAV is going to land. The contact forces raised during the landing maneuver are partially supported by the flexible link, causing a lateral deflection due to the weight of the aerial platform.

B. Impact Response

The goal of this experiment is to demonstrate that the long reach aerial manipulator is tolerant to impacts thanks to the passive joint of the pendulum. This simple mechanism brings two benefits w.r.t. the long reach manipulator presented in

[18]. On the one hand, the external wrenches exerted over the manipulator are not introduced as a torque in the pitch angle to the base of the multirotor, but as a force in the XZ-axes, so the propellers are less exposed to overloads. On the other hand, the pendulum acts as energy storage component (see Eq. (10) – (11)), in such a way that the energy associated to an impact in the aerial manipulator will be stored initially as potential energy by the manipulator through the rotation of the passive joint and the deflection of the compliant joints, transformed later into kinetic energy through the acceleration of the links, dissipated later by means of heat in the bearings.
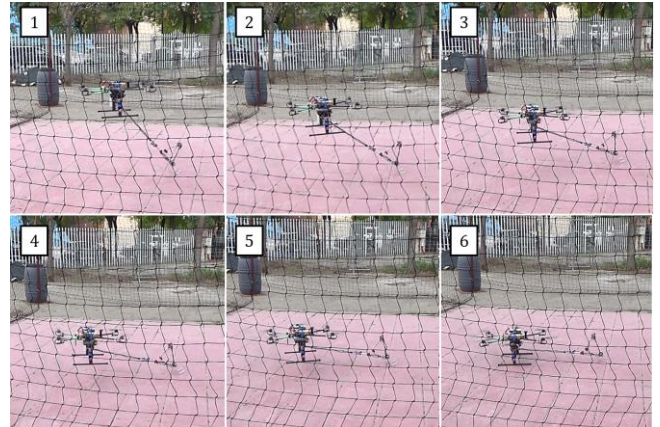

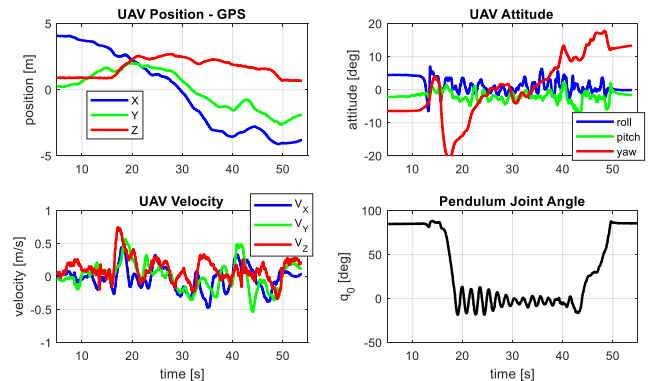Figure 8. Sequence of images corresponding to the landing operation.

Figure 9. Multirotor position, velocity, attitude, and pendulum rotation during the take-off and landing operation.

Figure 10 represents the position, velocity and orientation of the long reach aerial manipulator along with the rotation angle of the pendulum when this hits an obstacle at t = 160 s, while the aerial platform is moving at 2 m/s. The impact causes a 36° amplitude oscillation in the passive joint, which corresponds to a gravity potential energy of 1.3 J, considering the parameters indicated in Table 1. The oscillation remains 15 s, until it almost disappears. It is interesting to observe that the inertia of the aerial platform and the damping of the airflow tend to attenuate faster this oscillation than in the test-bench (Figure 14). The effect of the impact over the attitude controller can be seen in the Figure 10 as a 10° jump in the pitch angle at t = 160 s. The pilot reduced the velocity of the aerial platform just after the impact.
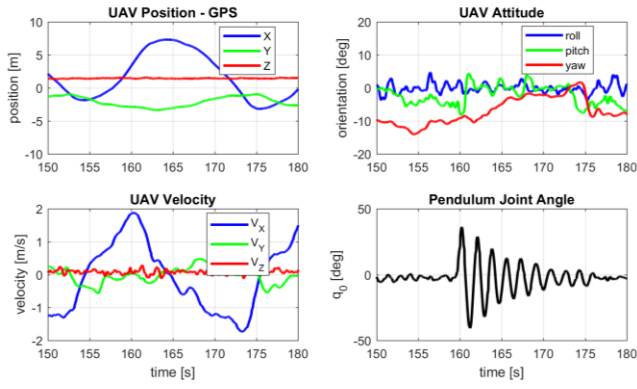
Figure 10. Multirotor position, velocity, attitude, and pendulum rotation when the tip of the long reach link hits an obstacle at t = 160 s while the hexarotor moves at 2 m/s, causing a 10 deg perturbation in the pitch angle.

C. Visual inspection with arm teleoperation

In this experiment, the compliant joint arm is teleoperated using the exoskeleton interface described in Section II-B and the visual display shown in Figure 11. In this task, the human operator has to approach and touch the base of a PVC pipe. The display shows a simplified model of the long reach aerial manipulator, including the joint angles and the distance given by the range sensor. Figure 12 represents the evolution of the signals during the operation. The feedback undershoots the reference due to the static deflection of the compliant joints (non-compensated gravity term). The maximum distance provided by the range sensor is around 500 mm, forcing its measurement to zero if the target object is out of range.
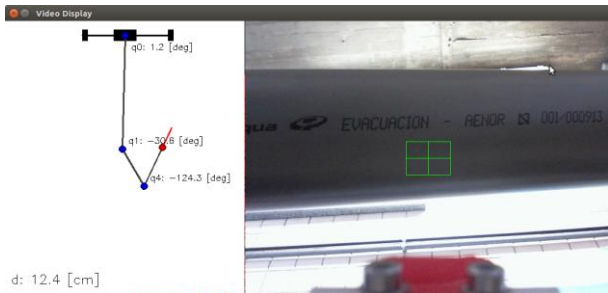

Figure 11. Visual display shown to the operator during the inspection task. The red line at the tip of the manipulator represents the distance to the pipe.
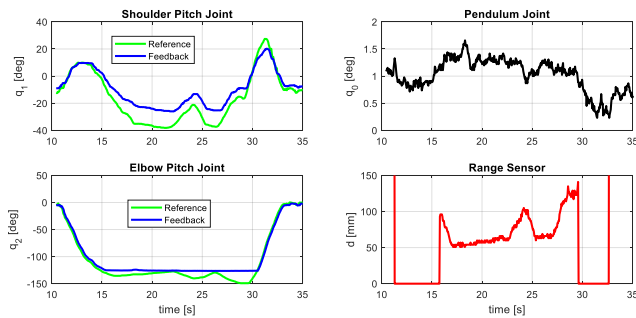

Figure 12. Joint position reference and feedback of the compliant arm (left), pendulum rotation (right, up) and range sensor (right, down) during the visual inspection of a pipe using the exoskeleton interface in test-bench.

It was found during the realization of the experiment that the visual representation of the LRM in the interface depicted in Figure 11 contributes to improve the situational awareness of the operator during the execution of the task, since it does not result intuitive to guide the motion of the arm using only the feedback provided by the eye-in-hand camera. The use of the exoskeleton interface also allows to replicate the motions of the operator in a more immediate and comfortable way.

D. Contact Force Control

The goal of this experiment is to validate the contact force control method described in Section IV-B based on Cartesian stiffness. Unlike reference [15], this implementation employs magnetic encoders to measure the deflection of the compliant joints, estimating the Cartesian deflection from the forward kinematics (Equation (17)) instead of using a vision sensor. In this test, the arm applies a 1 N pushing force in the X and Z axes consecutively while the base of the pendulum is fixed. Figure 13 shows the force reference and the estimation along with the joint angles and the evolution of the terms in the Cartesian stiffness matrix defined in Equation (18). The use of magnetic encoders improves significantly the performance of the force controller compared to the potentiometers used in [14] in terms of accuracy (0.2°), and in terms of rate (up to 1 kHz) compared to the vision sensor used in [15].
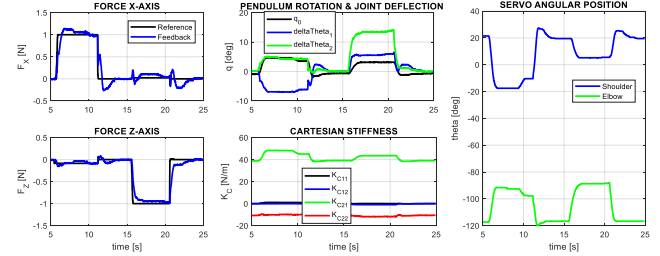

Figure 13. Contact force (left), joint deflection and servo angular position (middle) and Cartesian stiffness (right).

Two effects can be observed in Figure 13: 1) the variation of the Cartesian stiffness matrix depends on the servo angular position, since K_C depends on the Jacobian, and 2) the recoil motion of the passive joint when the arm applies the pushing force. The force controller in Figure 7 is a PID with $K_p = 25\ mm/N$, $K_d = 0.2\ mms/N$, and $K_i = 30\ mm/Ns$.

E. Attenuation of Oscillations in the Passive Joint Pendulum

The arm attached at the tip of the long reach link can contribute to attenuate the oscillations in the passive joint of pendulum, caused by impacts or accelerations of the aerial platform. Since the mass/inertia of the LRM is much higher than the mass/inertia of the compliant arm, it is expected that the arm requires more than one period to completely cancel the oscillation in the passive joint. This can be interpreted in terms of kinetic and potential energy (Equations (10)–(11)), evaluating the energy within a period. The motion of the UAV and the arm could be coordinated for a more efficient control, although this is out of the scope of this paper.

The vibration suppression method described in ref. [18] is applied here to attenuate the oscillations in the pendulum. The method consists of determining the maximum amplitude of the oscillation within a semi-period, q_0^{max}, detect the zero cross (that is, the time instant in which the phase of q_0 is zero or π rad), and generate a reaction motion with the shoulder joint with the same phase, so the reaction force associated to

the rotation of q_1 tends to cancel the oscillation of q_0. The amplitude of the reaction motion with the shoulder joint is proportional to the maximum amplitude of q_0 (gain K). As it can be seen in Figure 14, the free oscillation of the passive joint corresponds to a sinusoidal signal of period $T_0 = 2.1\ s$, damping coefficient $d_0 = 0.05\ s^{-1}$ and initial amplitude $Q_0 = 30\ deg$. Figure 13 also evidences that the oscillation is attenuated faster for higher values of gain K,. The reaction motion of the shoulder joint servo starts when the zero cross is detected, and it ends when the amplitude of the oscillation is maximum, that is, $T_0/4$ seconds later.
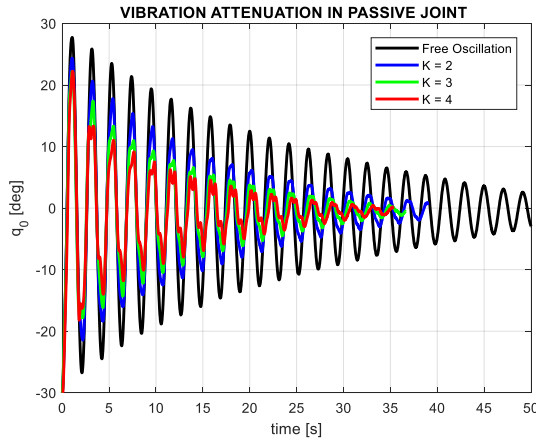

Figure 14. Rotation of the passive pendulum: free oscillation (black) and vibration attenuation using the arm with different compensation gains.

VI. CONCLUSION

This paper presented a new prototype of long reach aerial manipulator consisting of a 2-DOF compliant arm attached at the tip of a one meter length flexible link that rotates freely with respect to the base of a hexarotor platform, similarly to a passive pendulum. The motivation for this configuration is increasing the distance of the aerial platform to the obstacles in the workspace during the operation on flight, so the reaction time is higher, and thus the safety is improved. The developed prototype is intended to inspection tasks in areas of difficult access, facilitating its operation using a wearable exoskeleton interface with visual feedback display. The paper has demonstrated the possibility to perform the take-off and landing maneuvers in outdoors, evaluating also the tolerance to impacts with obstacles in the environment provided by the passive joint.

It is proposed as future work the development of a method to control the deflection in the flexible link using force or vision sensors placed at the base of the pendulum. The goal is to control the trajectories of the aerial manipulator taking into account the oscillation of the passive joint and the deflection of the link, exploiting the dynamic model for this purpose.

REFERENCES

[1] M. Fumagalli, R. Naldi, A. Macchelli, F. Forte, A. Keemink, S. Stramigioli, R. Carloni and L. Marconi, "Developing an aerial manipulator prototype: physical interaction with the environment," in *IEEE Robotics & Autom. Magazine*, vol. 21, no. 3, pp. 41-50, 2014.

[2] K. Alexis, G. Darivianakis, M. Burri and R. Siegwart, "Aerial robotic contact-based inspection: planning and control", in *Autonomous Robots,* vol. 40, pp. 631–655, 2016.

[3] M. Orsag, C. Korpela, S. Bogdan and P. Oh. Valve turning using a dual-arm aerial manipulator, *2014 International Conference on Unmanned Aircraft Systems (ICUAS)*, Orlando, FL, 2014, pp. 836-841

[4] C. Korpela, M. Orsag, and P. Oh, Towards valve turning using a dual-arm aerial manipulator. In Intelligent Robots and Systems (IROS 2014), 2014 IEEE/RSJ International Conference on (pp. 3411-3416).

[5] S. Kim, H. Seo and H. J. Kim, "Operating an unknown drawer using an aerial manipulator", in *IEEE International Conference on Robotics and Automation* (ICRA), May 2015, pp. 5503–5508.

[6] AEROARMS Project Home Page: http://aeroarms-project.eu.

[7] A. Suarez, P. R. Soria, G. Heredia, B. C. Arrue and A. Ollero, "Anthropomorphic, compliant and lightweight dual arm system for aerial manipulation," *2017 IEEE/RSJ Int. Conf. on Intelligent Robots and Systems (IROS)*, Vancouver, BC, 2017, pp. 992-997.

[8] C. D. Bellicoso, L. R. Buonocore, V. Lippiello and B. Siciliano. Design, modeling and control of a 5-DoF light-weight robot arm for aerial manipulation, *2015 23rd Mediterranean Conference on Control and Automation (MED)*, Torremolinos, 2015, pp. 853-858, 2011 IEEE/RSJ International Conference on (pp. 2668-2673). IEEE.

[9] K. Kondak, F. Huber, M. Schwarzbach, M. Laiacker, D. Sommer, M. Bejar, and A. Ollero. Aerial manipulation robot composed of an autonomous helicopter and a 7 degrees of freedom industrial manipulator, *2014 IEEE International Conference on Robotics and Automation (ICRA)*, Hong Kong, 2014, pp. 2107-2112.

[10] T. Tomić and S. Haddadin. A unified framework for external wrench estimation, interaction control and collision reflexes for flying robots, *2014 IEEE/RSJ International Conference on Intelligent Robots and Systems*, Chicago, IL, 2014, pp. 4197-4204.

[11] F. Ruggiero, J. Cacace, H. Sadeghian and V. Lippiello. Impedance control of VToL UAVs with a momentum-based external generalized forces estimator*, 2014 IEEE International Conference on Robotics and Automation (ICRA)*, Hong Kong, 2014, pp. 2093-2099.

[12] B. Yüksel, S. Mahboubi, C. Secchi, H. H. Bülthoff, and A. Franchi, "Design, identification and experimental testing of a light-weight flexible-joint arm for aerial physical interaction," In *Robotics and Automation (ICRA), 2015 IEEE Int. Conf. on* (pp. 870-876). IEEE.

[13] T. Bartelds, A. Capra, S. Hamaza, S. Stramigioli, and M. Fumagalli, "Compliant aerial manipulators: Toward a new generation of aerial robotic workers," 2016 *IEEE RAL*, *1*(1), 477-483.

[14] A. Suarez, G. Heredia, and A. Ollero, Lightweight compliant arm with compliant finger for aerial manipulation and grasping. In Intelligent Robots and Systems (IROS), 2016 IEEE/RSJ International Conf. on.

[15] A. Suarez, G. Heredia, A. Ollero, "Physical-virtual impedance control in ultra-lightweight and compliant dual arm aerial manipulators," *2018 Robotics and Automation Letters*.

[16] M. Manubens, D. Devaurs, L. Ros and J. Cortés. Motion planning for 6-D manipulation with aerial towed-cable systems. *Robotics: Science and Systems (RSS)*, Berlin, Germany, 2013

[17] H-N. Nguyen, S. Park, J. Park, and D. J. Lee. "A novel robotic platform for aerial manipulation using quadrotors as rotating thrust generators". *IEEE Transactions on Robotics*, in press, 2018.

[18] A. Suarez, A. M. Giordano, K. Kondak, G. Heredia, and A. Ollero, "Flexible long reach manipulator with lightweight dual arm: soft collision detection, reaction, and obstacle localization", in RobotSoft, 2018.

[19] A. Suarez, A. E. Jimenez-Cano, V. Vega, G. Heredia, A. Rodriguez-Castaño, and A. Ollero. (2018). Design of a lightweight dual arm system for aerial manipulation. *Mechatronics*, *vol 50*, pp. 30–44.

[20] D. W. Gu, P. Petkov, and M. M. Konstantinov, Robust control design with MATLAB®," 2005, Springer Science & Business Media.